

The GLAST Burst Monitor

Andreas von Kienlin^a, Charles A. Meegan^b, Giselher G. Lichti^a, Narayana P. Bhat^c, Michael S. Briggs^c, Valerie Connaughton^c, Roland Diehl^a, Gerald J. Fishman^b, Jochen Greiner^a, Andrew S. Hoover^d, R. Marc Kippen^d, Chryssa Kouveliotou^e, William S. Paciesas^c, Robert D. Preece^a, Volker Schönfelder^a, Helmut Steinle^a, and Robert B. Wilson^b

^aMax-Planck-Institut für extraterrestrische Physik, PO Box 1312, D-85741 Garching, Germany

^bNASA/Marshall Space-Flight Center, 320 Sparkman Drive, Huntsville, AL 35812, USA

^cUniversity of Alabama, Huntsville, AL 35899, USA

^dLos Alamos National Laboratory, ISR-2, Mail Stop B244, Los Alamos, NM 87545, USA

^eUniversities Space Research Association, USA

ABSTRACT

The next large NASA mission in the field of gamma-ray astronomy, GLAST, is scheduled for launch in 2007. Aside from the main instrument LAT (Large-Area Telescope), a gamma-ray telescope for the energy range between 20 MeV and > 100 GeV, a secondary instrument, the GLAST burst monitor (GBM), is foreseen. With this monitor one of the key scientific objectives of the mission, the determination of the high-energy behaviour of gamma-ray bursts and transients can be ensured. Its task is to increase the detection rate of gamma-ray bursts for the LAT and to extend the energy range to lower energies (from ~ 10 keV to ~ 30 MeV). It will provide real-time burst locations over a wide FoV with sufficient accuracy to allow repointing the GLAST spacecraft. Time-resolved spectra of many bursts recorded with LAT and the burst monitor will allow the investigation of the relation between the keV and the MeV-GeV emission from GRBs over unprecedented seven decades of energy. This will help to advance our understanding of the mechanisms by which gamma-rays are generated in gamma-ray bursts.

Keywords: Gamma rays: bursts; Instrumentation: detectors; Techniques: spectroscopic; Space vehicles: instruments

1. INTRODUCTION

GRBs are one of the most fascinating research topics in astrophysics. Since their discovery 35 years ago by the Vela satellites in 1967,¹ this phenomenon is still not totally understood and explained. The first major breakthrough in this field was obtained with the BATSE detectors² on NASA's Compton Gamma Ray Observatory (CGRO) mission. In the nine years of the CGRO mission, about 3000 bursts were registered, which showed an isotropic distribution over the entire sky, but with a deficiency of weak bursts. It was the Italian/Dutch satellite BeppoSAX³ which revealed the cosmological nature of GRBs with the identification of the first X-ray afterglow in 1997,⁴ which triggered the first successful follow-up observation at optical wavelengths.⁵ This finally ruled out the Galactic population models. The redshifts obtained to date for about 36 GRBs range from 0.0085 to 4.511*. Observational evidence now strongly suggests that GRBs longer than 2 seconds are associated with hypernovae.⁶⁻⁸ The origin of shorter bursts is more of a mystery – one hypothesis is that they are associated with the mergers of compact binaries.

The study of γ -ray bursts is one of the scientific objectives of the GLAST mission. This was motivated by observations of γ -ray bursts in the high-energy range above 50 MeV by EGRET onboard CGRO: The delayed emission of γ -quanta more than 1 hour after the burst start time was unexpected. In GRB940217 a 18 GeV γ -event was found in this extended emission.⁹ This delayed emission is in contrast to the characteristics of most of the bursts observed in the BATSE energy range, which have only a maximum duration of several 100 sec.

Further author information: (Send correspondence to A. von Kienlin)

A. v. Kienlin: E-mail: azk@mpe.mpg.de, Telephone: +49 (0)89 30000-3514

C. A. Meegan: E-mail: charles.meegan@msfc.nasa.gov, Telephone: (256) 961-7694

G. G. Lichti: E-mail: grl@mpe.mpg.de, Telephone: +49 (0)89 30000-3536

*Table of GRBs with known redshifts: <http://www.mpe.mpg.de/~jcg/grbrsh.html>

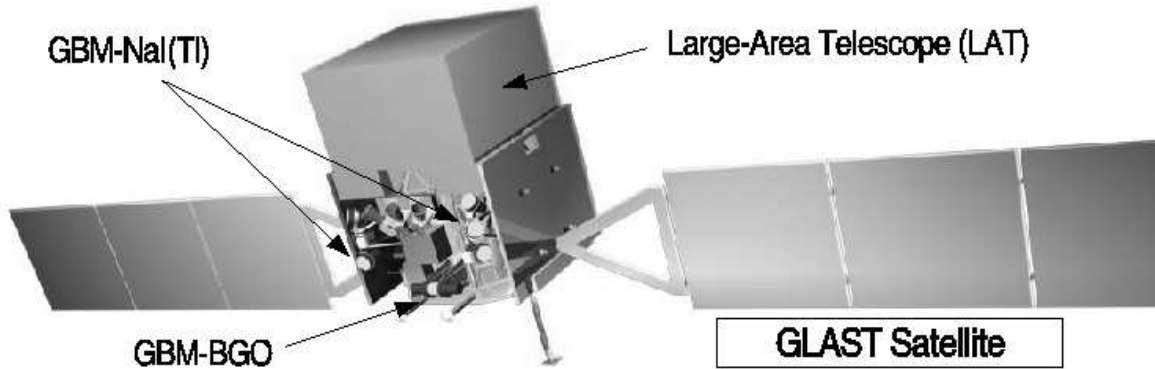


Figure 1. A schematic view of the GLAST satellite with the GLAST burst monitor (GBM). The 12 NaI(Tl)-detectors are mounted in 4 banks (the two banks on the back side are covered by the satellite), each equipped with 3 NaI(Tl)-detectors. The two BGO-detectors are mounted on opposite sides of the satellite. In contrast to the NaI(Tl)-detectors each BGO-detector is viewed by two PMTs.

The main instrument on GLAST, the Large-Area Telescope (LAT), will itself detect bursts with high sensitivity, and locate them with a precision of about 10 arcmin. Within several seconds LAT's burst locations can be relayed to ground- and space-based observatories to search for afterglow emission. The expected LAT burst trigger rate is between 50 and 100 bursts/year.

There are important limitations to the effectiveness of the LAT as a burst detector. High-energy measurements alone do not reveal the full physical picture. In the GRB energy spectra the most important characteristic currently known is a turnover or break (at break energy E_{break}) between two parts of the spectra, each described by a power law, with different spectral indices, with α as the low-energy power-law index and β as the high-energy power-law index¹⁰; this break occurs in the energy range between 100 and 500 keV, well below the LAT threshold of about 20 MeV. Furthermore, γ -ray bursts have their maximal luminosity around the break energy. The scientific return of the GLAST mission in the case of γ -ray bursts will be increased substantially by having simultaneous knowledge of the burst emission from GeV down to a few keV. This will help to answer the open questions of the relation between the high- and low-energy emission and especially the question if the high-energy γ -rays are a part of the burst-emission process itself or a kind of afterglow.

The GLAST Burst Monitor (GBM), which is able to cover the whole low-energy part of the γ -ray burst emission down to about 10 keV and simultaneously overlapping the lower part of the LAT energy range, will augment the capabilities of the LAT for γ -ray bursts. One of the important goals of the GBM is the continuation of the BATSE burst data base. A significant concern for GLAST as a burst detector are the technical problems associated with triggering, rapid source location and dead time. With GBM as an auxiliary, autonomous instrument these limitations will be mitigated.

The development and fabrication of the NaI(Tl)- and BGO-detector modules and the power supplies (LVPS, HVPS) is under the responsibility of MPE/DLR[†]. The MSFC/UAH group is responsible for the development of the Data Processing Unit (DPU), hard- and software and the project management.

2. INSTRUMENT DESCRIPTION AND DETECTOR DESIGN

GBM consists of 12 thin NaI(Tl)-plates, which are sensitive in the energy range between ~ 10 keV and ~ 1 MeV. Two additional BGO detectors, which are able to detect gamma-rays in the energy range between 150 keV and 30 MeV, are responsible for the overlap in energy with the LAT main instrument.

The 12 NaI(Tl) and 2 BGO scintillation detectors are mounted on the spacecraft as shown in Figure 1. The normals to the crystal discs of the 12 NaI(Tl) detectors are oriented in the following manner: six crystals in the

[†]Allocation of funds by DLR: Deutsches Zentrum für Luft- und Raumfahrt (German Aerospace Center).

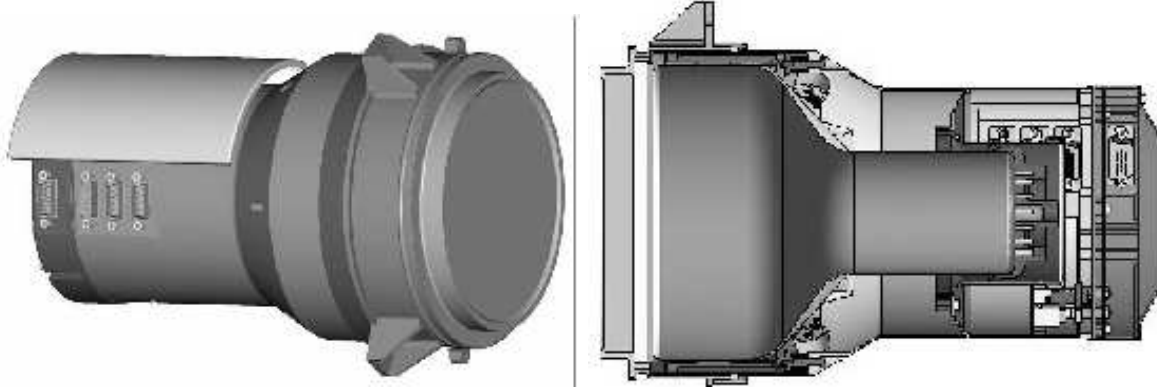


Figure 2. Side view and cross-section of one of the 12 NaI(Tl)-detector modules.

equatorial plane (hexagonal), four crystals at 45° (on a square) and two crystals at 20° (on opposite sides). This arrangement results in a large field of view for the GBM of > 8 sr and gives the opportunity for locating the origin of the burst by comparing the count rates of different NaIs (same method as used by BATSE). The two BGO detectors will be mounted on opposite sides of the spacecraft, providing nearly a 4π sr field of view.

Fig. 2 presents the design of the NaI(Tl) detector unit. These detectors consist of circular crystal disks made from NaI(Tl) each disk having a diameter of 127 mm (5 inch) and a thickness of 12.7 mm (0.5 inch). For light tightness and for sealing the crystals against atmospheric moisture (NaI(Tl) is very hygroscopic) each crystal is packed light-tight and in a hermetically sealed Al-housing (with the exception of the glass window to which the Photomultiplier Tube (PMT) is attached). In order to allow the measurement of X-rays down to 5 keV, the radiation entrance window is made of a 0.2 mm thick Beryllium sheet. Opposite to the Be sheet a circular glass plate covers and seals the crystals. The inner sides of the packing material have a reflective white cover in order to increase the light output of the crystals.

For the use in the GBM detectors the phototube R877 of Hamamatsu was selected. This tube was modified (R877RG-105) in order to fulfill the mechanical load-requirements for GBM. It is a head-on 5-inch diameter phototube made from borosilicate glass with a bi-alkali (CsSb) photocathode. It is a tube with a box/grid dynode structure with 10 stages. This tube has a well defined single-electron response and is therefore well-suited for detection down to very low energies. It has a good stability with temperature, count rate and time. Each PMT is shielded against magnetic fields with 0.125 mm thick Mumetal sheets, glued directly onto the glass tube. A second set of Mumetal sheets is attached to the PMT- and crystal-housing, which is further improving the magnetic shielding. The voltage divider, which is responsible for the supply of the dynode voltages, is mounted inside the PMT housing directly behind the feedthrough of the electrical leads. The collection efficiency of the photoelectrons is improved by using a divider ratio of 2:2:1:1...1, which increases the voltage drop between the photocathode, grid and first dynode. The front end electronic box (FEE box), utilizing a charge-sensitive amplifier (CSA), pulse-shaping circuits & line drivers, is mounted on the rear side of each detector module.

The two bismuth germanate (BGO) scintillators, are cylindrical in shape, with a diameter of 127 mm (5 inch) and a length of 127 mm (5 inch). The BGO cover shown in Fig. 3 is made of CFRP (Carbon Fibre Reinforced Plastic) with interface parts made of titanium. The thermal expansion coefficient of these two materials match well to the expansion coefficient of BGO. The CFRP wrapping is providing the light tightness and improving the mechanical stability of the BGO unit. In contrary to NaI(Tl) BGO is not hygroscopic. The two circular side windows of the crystal are polished in mirror quality. The cylindrical surface is roughened in order to guarantee a diffuse reflection of the generated photons. The circular crystal windows are viewed by two PMTs (same type as used for the NaI(Tl) detectors), this guarantees a better light collection and a higher level of redundancy. The anode signals of both PMTs are summed at the input stage of the DPU. The expected response of the NaI(Tl)- and BGO-detectors, expressed in effective area and energy resolution, is summarized in Figure 4.

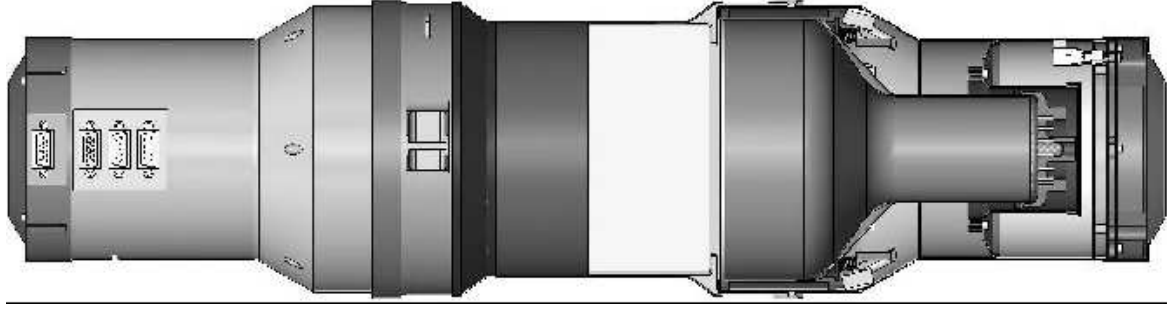


Figure 3. Side-view of the BGO detector unit. A bismuth germanate (BGO) scintillator-crystal, cylindrical in shape with a diameter of 127 mm (5 inch) and a length of 127 mm (5 inch), is viewed from both ends by a 5 inch PMT.

The arrangement and electrical interconnections of the different main elements of the GBM subsystem is shown in Fig. 5 as a block diagram. The 16 amplified PMT anode signals, 12 from the NaI(Tl) detectors and 2×2 from the BGO detectors, are fed to the DPU for digitalization. The DPU software will search for a significant increase in the counting rates from the detectors. In case of a positive detection, a burst alert will be generated and transmitted to ground and to the main instrument. The DPU will calculate from the count rates of the NaI(Tl)-detectors a rough direction of the burst and will deliver this information to the main instrument as well. The central High Voltage Power Supply HVPS, providing the high voltages for the 16 PMTs, and Low Voltage Power Supply LVPS, providing the supply voltages for the 16 FEEs and the DPU, are built-in in the central Power Box (PB). The HV level applied to each PMT is commanded by the DPU. Gain changes of the PMTs, caused by temperature changes and aging, can be balanced out by the DPU automatic gain-control algorithm, monitoring the 511 keV background line. Likewise Fig. 5 illustrates the areas of responsibilities of MPE/DLR, MSFC/UAH and GSFC/NASA.

3. EXPECTED GBM OUTPUT/RESULTS

The tasks of the GBM can be split up into three main topics each yielding an output important for various kinds of scientific analysis or for LAT support. The first output is certainly the GBM burst alert, which will be transmitted to LAT and ground. Next is the burst position, which will be provided by the GBM over a wide field of view. The last and most important output is the low-energy context measurement of the burst light curve and burst spectrum.

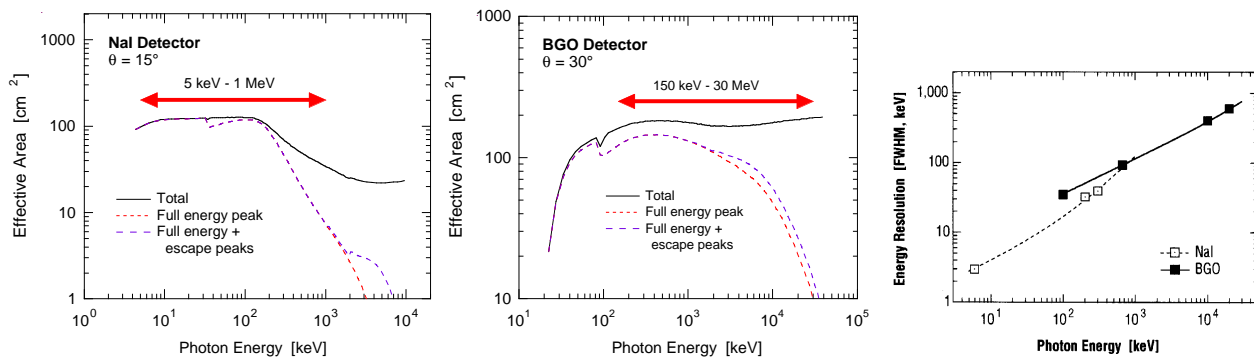


Figure 4. Effective area of a NaI(Tl)- and BGO-detector in dependence on the photon energy, with Θ as angle of incidence. The double arrow shows the energy range of the NaI(Tl) (left graph) and BGO (middle graph) detectors. The right graph shows the energy resolution of the NaI(Tl)- and BGO-detectors in dependence on the photon energy.

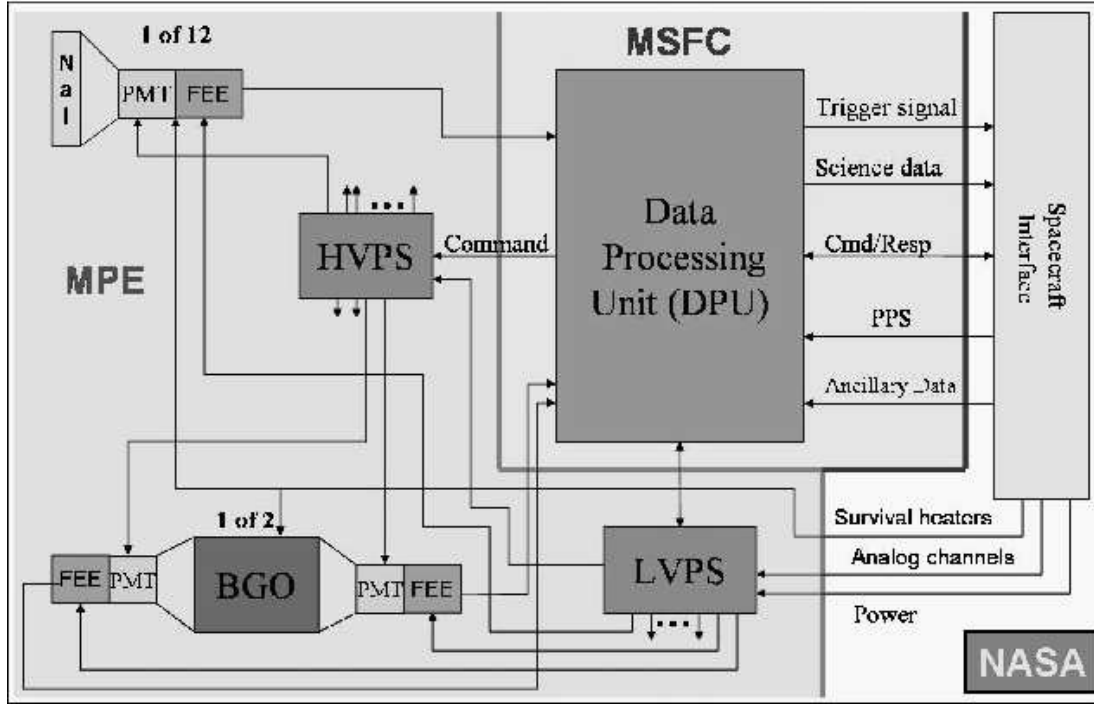


Figure 5. Block diagram of the main elements of the GBM subsystem. The responsibilities of MPE, MSFC and NASA are shown by different colours of the background.

3.1. GBM burst trigger

The trigger scheme for the GBM will be similar to that used with BATSE. The trigger requirement will be an excess in count rate above a threshold, specified in standard deviations above background, simultaneously for two of the NaI(Tl)-detector modules. The standard setting of the GBM threshold will be 4.5σ above background (energy interval: 50 keV to 300 keV, time interval for sensitivity calculations: 1.024 s). The requirement on the absolute on-board trigger sensitivity is < 1.0 photons $\text{cm}^{-2}\text{s}^{-1}$, with < 0.75 photons $\text{cm}^{-2}\text{s}^{-1}$ as a goal (BATSE at 5.5σ threshold: ~ 0.2 photons $\text{cm}^{-2}\text{s}^{-1}$). It is also planned to search on ground for fainter bursts using more sophisticated algorithms. One method is the summing of rates of closely pointing detectors and the inclusion of the BGO detector count rates. The current estimated sensitivity on ground is ~ 0.35 photons $\text{cm}^{-2}\text{s}^{-1}$ (5σ excess).

Based on the $\log N - \log P$ burst intensity distribution determined by BATSE¹¹ and considering the actual detector geometry, including the blockage by the LAT and spacecraft, the GBM will trigger on about 150-200 bursts per year. The estimated background level is based on BATSE rates and includes the effects of the variations due to altitude, latitude and longitude, and accounts for dead time due to transits through the South-Atlantic Anomaly (SAA). The simulation does not include the increased trigger rate one can expect by having additional triggering schemes that BATSE did not have, particularly the capability to trigger at lower energies.

3.2. GBM burst localization

The GBM determines locations of γ -ray burst by comparing count rates of NaI(Tl)-detectors, which are facing the sky in different directions. It is planned to increase the location accuracy in three stages: on board, automatic on ground and on ground manually. The burst location will be calculated on board in real time by the GBM-DPU, yielding an accuracy of about $< 15^\circ$ (1σ radius) within 1.8 s, which can be used as LAT trigger. If the burst occurred in the LAT field of view, data-reduction modes (reducing the LAT background by isolating the area of the GBM burst direction in the LAT dataspace) can be initiated in the LAT, which will increase

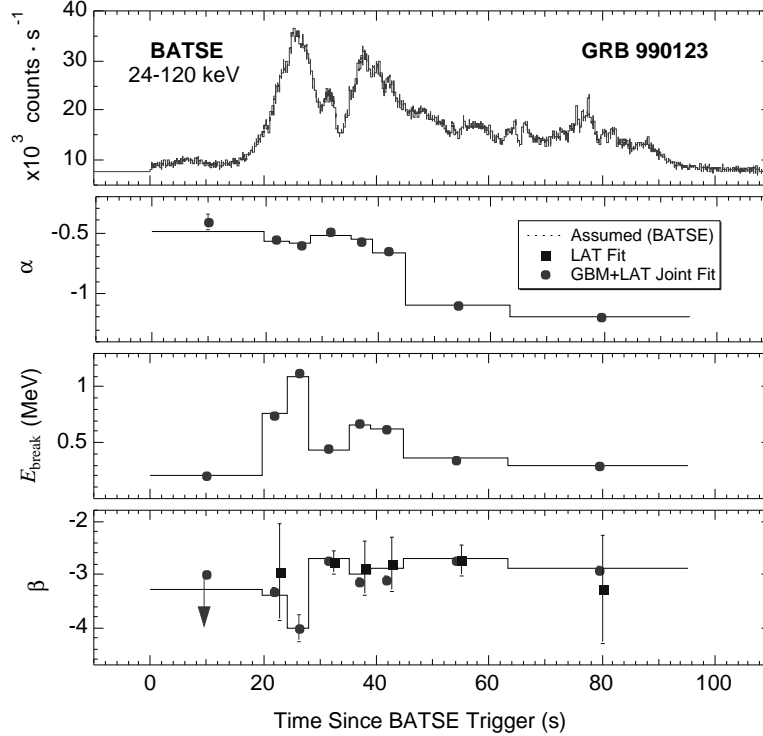


Figure 6. Time history of the simulated spectral parameters E_{break} , α and β using the data of GRB990123.

the LAT sensitivity for weak bursts. If the burst occurred outside the LAT field of view (FoV), the spacecraft can be repointed to observe delayed high-energy γ -ray emission. This is possible because the GBM FoV with > 8 sr is significantly larger than the LAT FoV with approximately 3 sr. After the transmission of the detector count rates to ground, the burst location can be computed with improved accuracy of less than 5° within 5 s. This will happen in near-real time (several seconds). This information can be used for the search of afterglow emission at other wavelengths, as input for the Gamma-ray burst Coordinates Network (GCN) and as input for the Interplanetary Network (IPN). The ground manual algorithms, which means a detailed analysis of the data with human interaction, will yield an improved burst location $< 3^\circ$ after one day.

3.3. GBM burst spectra and light curves

The burst monitor will provide time-resolved spectra and energy-resolved lightcurves in the energy range between 10 keV and 30 MeV, overlapping with the LAT lowest energy range (low-energy threshold at ~ 20 MeV). In order to fulfill the scientific goals the burst monitor will have four main data types. Two continuous data types are designed for burst analysis, for extremely long-lasting bursts, search for non-triggered events and for the detection of bright sources via the Earth-occultation technique. The first continuous data type accumulates 128 energy channels with 8.2 s time resolution for each detector and the second continuous data type 8 energy channels every 0.256 s. In response to a burst trigger, the GBM will produce a third datatype with high temporal resolution (2 μ s) and 128 channel spectral resolution. The fourth data type provides information on the burst location and spectral estimates determined on board.

3.4. Expected GBM results

Preliminary simulations of GBM and LAT data were performed to estimate the GRB measurement capability of the combined instruments. Fig. 6 shows the results of one such simulation, wherein the time-resolved spectral parameters of GRB 990123 measured with BATSE were used as inputs. This was one of the brightest bursts

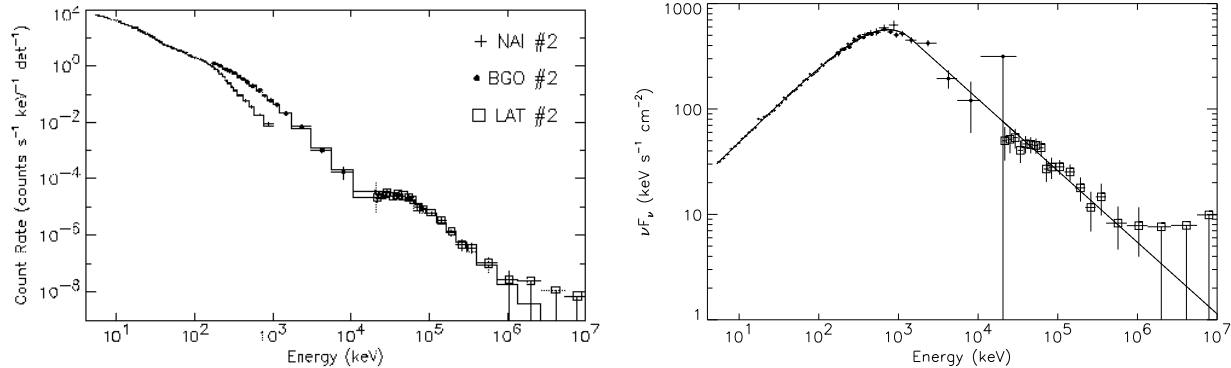


Figure 7. Simulated GBM-spectra using the data of GRB 940217 observed by BATSE, COMPTEL and EGRET.

detected with BATSE, having a fluence of 3×10^{-4} erg/ cm² (> 20 keV). Looking at the results for the β parameter one can see an excellent agreement, with small uncertainties, between the assumed BATSE values and the value derived from a common GBM/LAT fit. In comparison, the LAT-only fit shows large uncertainties, and provides no information at all about the α and E_{break} parameters. Fig. 7 shows the estimated response of the GBM together with the LAT to the time-integrated energy spectrum of GRB 940217 measured by the three CGRO instruments BATSE, COMPTEL and EGRET. The fluence of this burst was 7×10^{-4} erg/ cm² (> 20 keV). The simulated spectral data cover 6 energy decades from ~ 10 keV up to ~ 5 GeV. These examples indicate that the combination of GBM and LAT measurements promise to reveal the structure of prompt GRB spectra with unprecedented range and fidelity.

4. OUTLOOK

The GBM together with the LAT will help to improve our understanding of the central engines and emission mechanisms of γ -ray bursts. Till now it is not understood how the high-energy emission observed by EGRET is related to the low-energy emission. Even the production mechanisms for these energetic γ -rays has not been explained by current models. How can they escape the source region without being absorbed via γ - γ interaction with lower-energy photons? The GBM will help to uncover how bursts, observed with LAT in the GeV regime, fit into the whole population. It will also allow to link the LAT sample with the afterglow sample via the BATSE-like parameters. This is important, because the high-energy measurements alone do not allow a classification. It is one of the goals of the GBM team to produce a catalog of bursts that will include parameters such as location, duration, peak flux, and fluence, as well as spectral properties. These parameters will be defined as closely as possible to those in the BATSE catalog, so that the bursts observed by GLAST can be related to the large sample of the BATSE catalog. The continuation of the BATSE database will be one of the benefits of the GBM. In contrast to the simple spectral shape of bursts the observed temporal behaviour is varying strongly. Several common characteristic effects in the evolution of bursts have been observed, such as narrowing of pulses with increasing energy, a softening trend, and a hardness-intensity correlation. An interesting question for the GLAST mission will be how these temporal characteristics will behave when the energy band is increased. The investigation of the temporal behaviour and distribution of the spectral parameters (E_{break} , α , β and the correlation between E_{break} and the high-energy emission observed by the LAT) is one of the important tasks of the GBM. There are several other questions which will hopefully be answered with the help of GBM: In many spectra the power-law index β appears flatter than -2 . Such spectra cannot continue to infinitely high energies without steepening; an expected high-energy break may, in a few cases, be measured by the LAT alone. But in many cases the constraints will be improved by fitting a wide-band spectrum, including the GBM spectra. Another interesting question is whether there exists a significant population of hard-spectrum bursts which have been missed or poorly sampled by BATSE. GLAST can settle this question only by sufficient simultaneous coverage of the BATSE energy range. The good temporal resolution will make GLAST an excellent detector for the 4th GRB Interplanetary Network (IPN), too.

ACKNOWLEDGMENTS

The Glast Burst Monitor project is supported by the German "Ministerium für Bildung und Forschung" through DLR grant 50.QV.0301.

REFERENCES

1. R. W. Klebesadel, I. B. Strong, and R. A. Olson, "Observations of Gamma-Ray Bursts of Cosmic Origin," *ApJ* **182**, pp. L85+, June 1973.
2. G. J. Fishman, C. A. Meegan, R. B. Wilson, *et al.*, "The Burst and Transient Source Experiment on the Gamma Ray Observatory," in *Proc. GRO Science Workshop, April 10 - 12, 1989, Goddard Space Flight Center, Greenbelt, MD, USA*, W. N. Johnson, ed., pp. 2-39, GSFC, 1989.
3. G. Boella, R. C. Butler, G. C. Perola, L. Piro, L. Scarsi, and J. A. M. Bleeker, "BeppoSAX, the wide band mission for X-ray astronomy," *A&AS* **122**, pp. 299-307, Apr. 1997.
4. E. Costa, F. Frontera, J. Heise, M. Feroci, J. in 't Zand, F. Fiore, M. N. Cinti, D. dal Fiume, L. Nicastro, M. Orlandini, E. Palazzi, M. Rapisarda, G. Zavattini, R. Jager, A. Parmar, A. Owens, S. Molendi, G. Cusumano, M. C. Maccarone, S. Giarrusso, A. Coletta, L. A. Antonelli, P. Giommi, J. M. Muller, L. Piro, and R. C. Butler, "Discovery of an X-ray afterglow associated with the gamma-ray burst of 28 February 1997.," *Nature* **387**, pp. 783-785, 1997.
5. J. van Paradijs, P. J. Groot, T. Galama, C. Kouveliotou, R. G. Strom, J. Telting, R. G. M. Rutten, G. J. Fishman, C. A. Meegan, M. Pettini, N. Tanvir, J. Bloom, H. Pedersen, H. U. Nordgaard-Nielsen, M. Lindenvornle, J. Melnick, G. van der Steene, M. Bremer, R. Naber, J. Heise, J. in 't Zand, E. Costa, M. Feroci, L. Piro, F. Frontera, G. Zavattini, L. Nicastro, E. Palazzi, K. Bennet, L. Hanlon, and A. Parmar, "Transient optical emission from the error box of the gamma-ray burst of 28 February 1997.," *Nature* **386**, pp. 686-689, 1997.
6. T. J. Galama, P. M. Vreeswijk, J. van Paradijs, C. Kouveliotou, T. Augusteijn, H. Bohnhardt, J. P. Brewer, V. Doublier, J.-F. Gonzalez, B. Leibundgut, C. Lidman, O. R. Hainaut, F. Patat, J. Heise, J. in 't Zand, K. Hurley, P. J. Groot, R. G. Strom, P. A. Mazzali, K. Iwamoto, K. Nomoto, H. Umeda, T. Nakamura, T. R. Young, T. Suzuki, T. Shigeyama, T. Koshut, M. Kippen, C. Robinson, P. de Wildt, R. A. M. J. Wijers, N. Tanvir, J. Greiner, E. Pian, E. Palazzi, F. Frontera, N. Masetti, L. Nicastro, M. Feroci, E. Costa, L. Piro, B. A. Peterson, C. Tinney, B. Boyle, R. Cannon, R. Stathakis, E. Sadler, M. C. Begam, and P. Ianna, "An unusual supernova in the error box of the gamma-ray burst of 25 April 1998.," *Nature* **395**, pp. 670-672, 1998.
7. K. Z. Stanek, T. Matheson, P. M. Garnavich, P. Martini, P. Berlind, N. Caldwell, P. Challis, W. R. Brown, R. Schild, K. Krisciunas, M. L. Calkins, J. C. Lee, N. Hathi, R. A. Jansen, R. Windhorst, L. Echevarria, D. J. Eisenstein, B. Pindor, E. W. Olszewski, P. Harding, S. T. Holland, and D. Bersier, "Spectroscopic Discovery of the Supernova 2003dh Associated with GRB 030329," *ApJ* **591**, pp. L17-L20, July 2003.
8. J. Hjorth, J. Sollerman, P. Møller, J. P. U. Fynbo, S. E. Woosley, C. Kouveliotou, N. R. Tanvir, J. Greiner, M. I. Andersen, A. J. Castro-Tirado, J. M. Castro Cerón, A. S. Fruchter, J. Gorosabel, P. Jakobsson, L. Kaper, S. Klose, N. Masetti, H. Pedersen, K. Pedersen, E. Pian, E. Palazzi, J. E. Rhoads, E. Rol, E. P. J. van den Heuvel, P. M. Vreeswijk, D. Watson, and R. A. M. J. Wijers, "A very energetic supernova associated with the γ -ray burst of 29 March 2003," *Nature* **423**, pp. 847-850, June 2003.
9. K. Hurley, "Detection of a Gamma-Ray Burst of Very Long Duration and Very High Energy," *Nature* **372**, p. 652, 1994.
10. D. Band, J. Matteson, L. Ford, B. Schaefer, D. Palmer, B. Teegarden, T. Cline, M. Briggs, W. Paciesas, G. Pendleton, G. Fishman, C. Kouveliotou, C. Meegan, R. Wilson, and P. Lestrade, "BATSE observations of gamma-ray burst spectra. I - Spectral diversity," *ApJ* **413**, pp. 281-292, 1993.
11. W. S. Paciesas, C. A. Meegan, G. N. Pendleton, M. S. Briggs, C. Kouveliotou, T. M. Koshut, J. P. Lestrade, M. L. McCollough, J. J. Brainerd, J. Hakkila, W. Henze, R. D. Preece, V. Connaughton, R. M. Kippen, R. S. Mallozzi, G. J. Fishman, G. A. Richardson, and M. Sahi, "The Fourth BATSE Gamma-Ray Burst Catalog (Revised)," *ApJS* **122**, pp. 465-495, June 1999.